Segmentation of Vessels: The Corkscrew Algorithm

Stefan Wesarg, and Evelyn A. Firle

Fraunhofer IGD, Cognitive Computing & Medical Imaging, Darmstadt, Germany

ABSTRACT

Medical imaging is nowadays much more than only providing data for diagnosis. It also links 'classical' diagnosis to modern forms of treatment such as image guided surgery. Those systems require the identification of organs, anatomical regions of the human body etc., i. e. the segmentation of structures from medical data sets. The algorithms used for these segmentation tasks strongly depend on the object to be segmented.

One structure which plays an important role in surgery planning are vessels that are found everywhere in the human body. Several approaches for their extraction already exist. However, there is no general one which is suitable for all types of data or all sorts of vascular structures.

This work presents a new algorithm for the segmentation of vessels. It can be classified as a skeleton-based approach working on 3D data sets, and has been designed for a reliable segmentation of coronary arteries. The algorithm is a semi-automatic extraction technique requirering the definition of the start and end the point of the (centerline) path to be found. A first estimation of the vessel's centerline is calculated and then corrected iteratively by detecting the vessel's border perpendicular to the centerline.

We used contrast enhanced CT data sets of the thorax for testing our approach. Coronary arteries have been extracted from the data sets using the 'corkscrew algorithm' presented in this work. The segmentation turned out to be robust even if moderate breathing artifacts were present in the data sets.

Keywords: Segmentation, vessel extraction, medical imaging, computed tomography, cardiology, coronary arteries

1. INTRODUCTION

Nowadays, medical images are provided by several imaging modalities. The employment of the acquired image data allows a differentiation into diagnostic imaging and intra-operative imaging. Diagnostic imaging is the 'traditional' application of such data. Based on the information extracted from it diseases are identified and an adequate treatment is planned. For instance, in radiation therapy that treatment planning plays a key role for a successful delivery of the dose. But, over the last two decades a new trend concerning the usage of medical image data could be perceived. That data is not only employed for diagnosis anymore but also during interventions. This intra-operative imaging led to a new treatment form called 'image-guided surgery' using medical navigation systems.

However, the acquired image data does not provide directly all the information required for accomplishing the above tasks. Here, image processing comes into play revealing details from the images that have been hidden inside but that are representing valuable, additional information. Today, typical image processing tasks like windowing, setting transparency, and basic filtering are already integrated into the imaging software that is

E-mail: (Send correspondence to S.W.)
S. W. : stefan.wesarg@igd.fraunhofer.de
E. A. F. : evelyn.firle@igd.fraunhofer.de

delivered with the devices for the image acquisition. But, the recognition of important structures can still be facilitated if they are highlighted or in any other way visually accentuated. This requires a segmentation of these structures from the image data which means in fact a binary classification of the voxels representing the image data into those being part of the structure and those not belonging to it. In addition to the possibility of enhancing the visualization, the segmentation of anatomical objects also allows an improved analysis of them. This can be, for instance, the detection of abnormalities of shape or functionality.

2. MOTIVATION

Heart disease and malfunction of the cardiovascular system is the most frequent cause of death in the developed nations. In addition to problems related to the myocardium often a disfunction of coronary arteries causes severe risks for the patient's health. An established procedure for the treatment of illness due to calcified coronary arteries is the bypass grafting. The availabilty of new technology currently changes the way of how such operations are executed in a dramatic manner. The usage of so-called 'telemanipulators' allows that the intervention can be executed as a special form of minimal-invasive surgery. During such a totally endoscopic coronary artery bypass (TECAB) grafting[1] the chest is no longer completely opened, and the intervention can be done on a beating heart. In order to bring the instruments and the endoscope to the operation area above the heart, ports have to be set, representing the entry points for the instruments.

Within the project MEDARPA[2] an innovative augmented reality (AR) system for supporting minimal-invasive interventions has been developed. One medical scenario it is tested with is the port placement for those TECAB grafting. The transparent display being the core component of the system serves in combination with a tracked pointing device as a 'magic window' allowing a look inside the patient by providing an overlay of anatomical image data in front of the operation area. (For more information see references.[3–6])

An exact knowledge about the patient's anatomy is mandatory since this interventional treatment method is used when stenoses due to strongly calcified coronary arteries are present. In that case the calcified segments block the vessel and disturb the blood flow. To compensate for that problem a vessel segment from the patient's leg is attached with one end before and the other one after the calcified part of the coronary artery, allowing the blood flow towards the heart's apex region again. Here, a segmentation of the vessel allows for a better planning of the intervention and simplifies the diagnosis particularly if additional information based on the segmentation result is extracted.[7]

3. EXISTING VESSEL SEGMENTATION APPROACHES

Over the past years various approaches for segmenting vessels in medical image data have been published. A detailed review and a classification of these techniques can be found on the internet.[8] Existing approaches differ on one hand in their fundamental attempt to the segmentation problem and on the other hand in the imaging modality they have been tested with.

A common imaging modality used for the examination of the vascular system is angiography. This technique, being established as X-Ray and MR angiography, acquires 2D projection images. For a better visibility the vessels are often contrast-enhanced. The segmentation problem in that case is then reduced to a segmentation of high intensity curves in front of a dark background from a 2D slice. Combining projection images acquired from different view positions including the segmentation results allows for the 3D reconstruction of the vascular structure.[9, 10]

Other techniques work on 3D data sets deliverd by CT or MR scanners. There, algorithms truely working in 3D space are required. They differ in the segmentation result depending on the intended usage of that output. Some of the algorithms extract only the vessel's centerline[11] whereas others deliver the vessel's surface,[12] and some of them even both.[13, 14] Furthermore, the different approaches vary in the ability whether they can handle bifurcations[11, 12] or not.[14, 15] Finally, most of the algorithms are designed for a special segmentation purpose like segmenting the bronchus tree[11] or reconstructing cerebral vessels.[16]

Verdonck et al.[13] proposed a technique they called the 'imaginary catheter'. This tracking-based approach segments the vessel by moving the 'catheter's' tip forward along the estimated centerline and detects its border

searching along a set of rays perpendicular to the centerline. According to the considered segment of the search path, the volume has to be resliced continuously which represents a time-consuming task associated with possible interpolation artifacts. Their algorithm extracts the vessel's centerline as well as its border, and has been tested with spiral CT and MR angiography data.

Kawata et al.[15] developed an algorithm for the detection of blood vessel diseases based on cone-beam CT data. Their work has been focused on the detection of abnormalities in morphology based on developed surface representations for aneurysms and stenoses.

A detection technique for tracheal stenoses has been introduced by Sorantin et al..[14] An automatic segmentation of the laryngo-tracheal tract is followed by a skeltonization algorithm computing the trachea's centerline. In addition, they created line charts showing degree and length of the stenoses. However, the trachea's diameter is much greater than that of the most blood vessels.

The corkscrew algorithm presented in this work has been designed for segmenting coronary arteries. It has been tested with contrast-enhanced CT data sets of the thorax. Our technique is working in 3D, and extracts the vessel's centerline as well as its border. Following the above mentioned review on vessel extraction techniques[8] our algorithm can be classified as a skeleton-based approach employing mathematical morphology schemes. This characterizes it as a pattern recognition technique. However, due to its iterative correction of the vessel's centerline in combination with the detection of its border, the algorithm presented in this work can also be considered as a tracking-based approach.

4. MATERIAL AND METHODS

This section presents our 'corkscrew algorithm' in detail. Its design has been focused on the extraction of coronary arteries from CT data sets for supporting the planning of the TECAB grafting (see section 2) as well as the intra-operative imaging during the port placement. This lead to some constraints being discussed in the following. Afterwards, the steps of the algorithm are presented.

4.1. DESIGN CONSTRAINTS FOR THE ALGORITHM

For the planning of a TECAB grafting, image data using a CT scanner is acquired. In order to improve the visibility of the coronary arteries, contrast agents are applied directly into the heart resulting in a higher attenuation of the photons in areas where the contrast agent is present. This leads to higher Hounsfield values and therefore an easier perception of these cardiovascular structures, since they are brighter than the surrounding tissue. As a consequence of that image acquisition technique, the algorithm has to be designed for the detection of structures, that are relative bright and homogeneous tubular objects, in high-resolution image data sets.

The preparation of the intervention by the surgeon comprises also a decision about the location of the cuts for the connection of the bypass. We use these two positions as an input for the start and end point of the segmentation routine.

An additional analysis of the coronary artery's segment could reveal useful information for the planning of the intervention. That is why a segmentation of the vessel's centerline as well as its border is required. Stenoses due to existing calcifications can easier by detected in the case of excluding calcified regions from the segmentation result, since that decreases the vessel's diameter in those regions. Therefore, the algorithm should correctly handle such areas, and segment only that part of the artery where the blood can pass.

Based on these demands the following design constraints for the segmentation algorithm can be defined:

- A 3D segmentation of coronary arteries in contrast-enhanced CT data sets has to be done.

- The segmentation has to be carried out based on the user defined start and end point. → The algorithm has to work semi-automatically.

- The computation output has to provide the centerline and the border of the vessel.

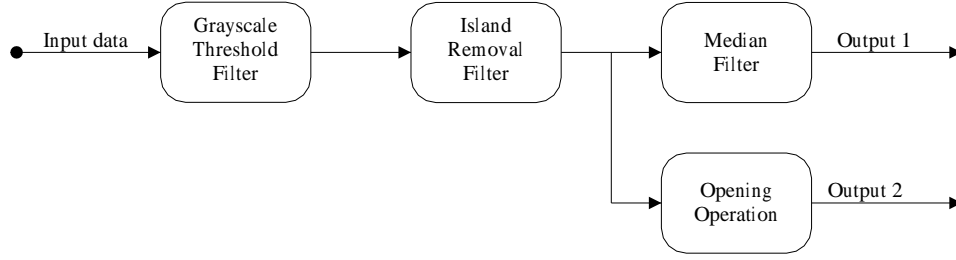- Calcifications have to be excluded from the segmented region.

Figure 1. The filter chain used for the pre-processing of the image data. Two output data sets are generated for the subsequent steps of the segmentation algorithm.

The usage of contrast-enhanced CT image data simplifies the segmentation task since on one hand the vessel appears relatively bright with respect to the surrounding tissue, and on the other hand the used contrast agent causes a homogeneous brightness along the vessel. In addition, the Hounsfield value of a calcification that may be present is still higher than that of the contrast-enhanced vessel. Due to the fact that coronary arteries are small in diameter (approx. 2 to 3 mm) and a resolution of the image data of approx. 0.5 mm, side branches of the vascular structure to be segmented are in the range of the detection threshold given by the imaging modality resp. the imaging device. Thus, in conjunction with the need for extracting only segments of coronary arteries a special handling of bifurcations is not required.

These design constraints led us to a three-step approach for the vessel segmentation, consisting of a pre-processing, a first estimation of the centerline, and its iterative correction in combination with the border detection

4.2. PRE-PROCESSING OF THE IMAGE DATA

The pre-processing, executed at the beginning of our proposed segmentation technique, is made up of a number of filters, commonly used in image processing. The output of this step should facilitate the detection of the centerline and the border in the subsequent steps. Our filter chain utilizes the user defined start point for accessing the voxel's gray value at that position. In detail, it runs as follows (see figure 1):

1. A seeded grayscale thresholding is executed slice by slice using the gray value at the start point for defining a lower and upper threshold based on 90% and 110% of that value. This filter sets all voxels' values to 0 if they are outside that range. Voxels with values between the lower and the upper threshold remain unchanged.

2. Small spots inside the regions with values greater than zero are set to the value of their 2D neighborhood by applying an island removal filter to the output of the preceding step.

3. A 2D median filter is applied to the output of the last step. The modified value at the start position is stored for later use.

4. The output of step 2 is taken as input for an opening operation in 2D. This ensures the exclusion of calcifications from the segmentation result (see figure 2).

Thus, the pre-processing results in two output data sets (steps 3 and 4). The first one controls the homogeneity of the vessel, and the second one the exclusion of calcifications in the subsequent segmentation steps.

4.3. FIRST ESTIMATION OF THE CENTERLINE

As a result of the initial pre-processing presented in the last section two output data sets are created (see section 4.2). They contain a slightly modified version of the thresholding filter's output due to the additional filters that have been applied. There, the object to be extracted – the coronary artery – is already pre-segmented, but the data sets still contain other structures with gray values according to the range calculated in step 1 of the pre-processing.
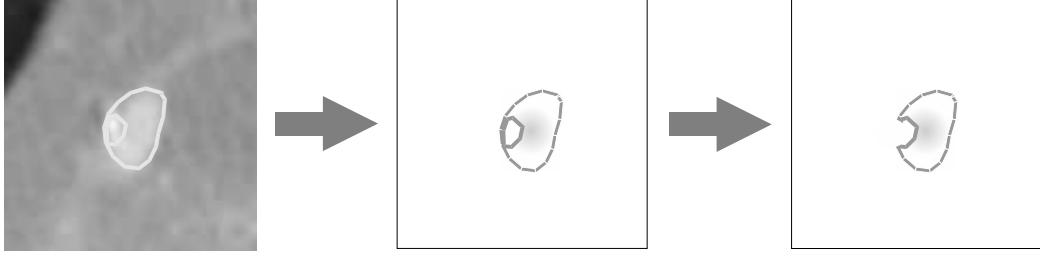
Figure 2. The opening operation applied after the grayscale threshold filter and the island removal filter eliminates possibly existing connections surrounding a calcified region inside the vessel: After the original image data (left image) has been filtered using a grayscale thresholding and island removal technique, the remaining structure is the vessel with a hole inside (middle image). The opening operation removes the vessel's border 'behind' the calcification (right image).

The current step generates a first estimation for the centerline by finding a path that connects the defined start and end point by traversing only voxels with a gray value greater than 0. Its special way of traveling results in a path formed like a helix – or a corkscrew – if a non-curved tubular object is examined. This path's generation is guided by a simple cost function taking the two input data sets of this step into account. That function's value at voxel position (x, y, z) is defined as

$$c_{vox}(x, y, z) = c_{med}(x, y, z) + c_{op}(x, y, z). \tag{1}$$

It contains two terms calculated from the output of the median filter (c_{med}) and the opening operation (c_{op}). These terms are defined using the gray values f_{med} and f_{op} at the corresponding voxel position (x, y, z), and the mean values i_{med} and i_{op} computed in the steps 1 and 3 of the pre-processing:

$$c_{med}(x, y, z) = \begin{cases} \infty & , g_{med}(x, y, z) > \alpha \\ g_{med}(x, y, z) & , g_{med}(x, y, z) \leq \alpha \end{cases} \quad , \quad c_{op}(x, y, z) = \begin{cases} \infty & , g_{op}(x, y, z) > \beta \\ g_{op}(x, y, z) & , g_{op}(x, y, z) \leq \beta \end{cases} \tag{2}$$

with

$$g_{med}(x, y, z) = \left| \frac{f_{med}(x, y, z) - i_{med}}{i_{med}} \right| \quad , \quad g_{op}(x, y, z) = \left| \frac{f_{op}(x, y, z) - i_{op}}{i_{op}} \right|. \tag{3}$$

The parameters α and β are freely adjustable values. But due to the values of 90% and 110% used for the grayscale thresholding in the pre-processing step (see section 4.2) a value of 0.1 for them both is a reasonable choice, leading to a reliable and robust segmentation result for a large range of data sets. Using that cost function, the first estimation of the centerline is generated as follows (see figure 3):

1. Using the differences between start and end point for each component x, y, and z, the 'preferred' direction for each axis is computed.

2. One of these 'preferred' directions (e.g. that parallel to the z axis) is set as initial direction for the search.

3. Move forward step by step along this direction until one of the terms in the the cost funtion (eq. 1) equals to ∞.

4. One step backwards in order to hold the found position for sure inside the vessel.

5. Compute new direction:

   (a) If the preceding direction was one of the 'preferred' directions for each axis (x, y, z) and last and current stop points (see 6) are different, then the new direction is the next 'preferred' direction which is given by cycling the axes $[\hookrightarrow x \rightarrow y \rightarrow z \rightarrow]$.

   (b) If same as 5a but last and current stop points are equal, then the new direction is the 'non-preferred' direction for the corresponding axis.
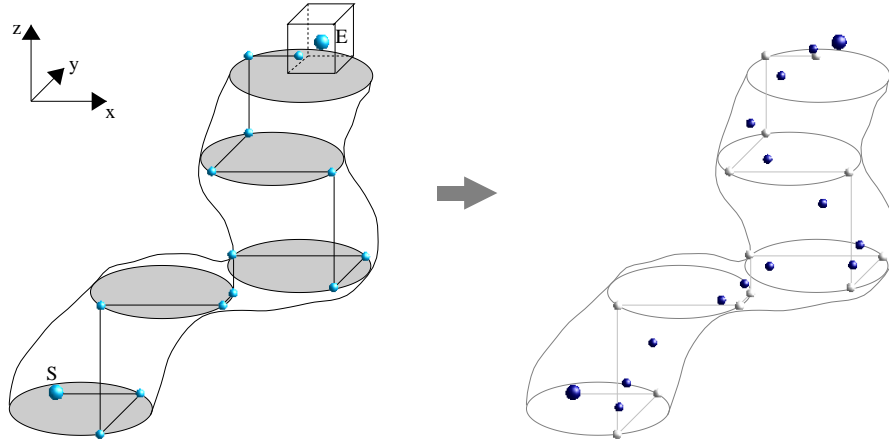
Figure 3. The search path of the corkscrew algorithm: The search direction is cycling the axes (x, y, z). If the search finds a border this position is stored and the search continues along the next axis. The search is stopped when the path enters a defined region around the end point (cube at the top).

The centers of gravity for each three subsequent 'stop points' are calculated. Start and end point of the search are added as well to that point list. This operation generates a list of points (dark colored) with positions deeper inside the vessel than the previous 'stop points' (bright colored).

      (c) If the last direction was one of the 'non-preferred' directions, then the new direction is the 'preferred' direction for the next axis.

6. Store current position ('stop point').

7. Repeat steps 3 to 6 until path is found.

8. Calculate the center of gravity for each subsequent three stop points respectively and store these points adding the user defined start and end point at the top resp. bottom of this list (see figure 3).

   In general, this search will not pass exactly the position of the end point defined by the user. Therefore, a region around the end point containing a few voxels in every direction (x, y, z) has to be defined. The search is terminated when it passes this region. The points generated in step 8 are used as control points for a B-spline interpolation. The resulting path is a first estimation of the vessel's centerline.

4.4. ITERATIVE BORDER DETECTION AND CENTERLINE CORRECTION

The point list generated in the preceding step contains coordinates for positions, that lie inside the vascular structure to be segmented, but they are not likely the points forming the 'real' centerline of the vessel. The last step of our segmentation algorithm corrects these positions by searching the points that form the vessel's border. The search is executed for every point of the list, generated during the last step, and then for the whole point list in an iterative manner. The number of iterations has to be given. Due to the border detection technique we used, the corkscrew algorithm can be considered as a tracking-based approach. In detail, that part of the algorithm is made up of the following steps:

1. The first estimation of the centerline (see section 4.3) and the pre-processing output data are taken as input.

2. Search the vessel's border in orthogonal direction to the segment of the (current) centerline. The search is executed on a number ν of equiangular lines, spreading out from the corresponding point of the centerline.

3. Compute the corrected position for each point of the (current) centerline using the positions of the border points from step 2 as follows (see figure 4):
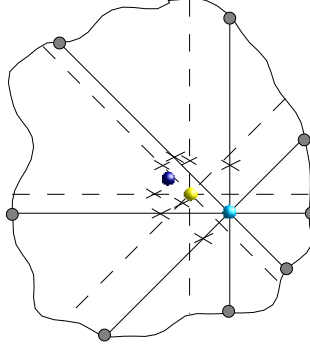
Figure 4. The iterative correction of the centerline position (shown for one plane othogonal to the centerline segment and 8 spreading lines). Each iteration moves the previous position closer to the center of the contour. The output of the second iteration (dark ball) is already much closer to the real center than the initial position.

     (a) Compute the center of gravity for each two opposite border points respectively.

     (b) Compute the center of gravity for all of the points computed in step 3a.

   4. The corrected centerline from step 3 is the modified input for step 2 and start iteration.

For deciding whether the border has been reached, we used the same cost function as defined in equation 1 in section 4.3. The parameter ν for the number of equiangular lines spreading out from every point of the current centerline can be freely selected. A too small value would result in a non-closed border, a too high one would unnecessarily increase the computation time.

The result of this iterative computation is a set of points defining the corrected centerline, and in addition a set of points forming the vessel's border. Based on the list of border points, the vessel's border can be visualized directly in the 2D slices. For visualizing that border in a 3D rendered scene of the volume, we generated a polygonal mesh using a marching cubes algorithm (see e. g. ref.[17]).

5. RESULTS

The 'corkscrew algorithm' has been tested with 12 data sets. That image data has been acquired using a multi-slice CT scanner (*Somatom Sensation 16*, Siemens). A contrast agent has been applied in all cases resulting in a bright appearance of the coronary arteries with respect to the surrounding tissue. The data sets consisted of between 205 and 295 slices with nearly cubic voxels of approx. $0.5\,mm$ length for each direction (x, y, z), covering between 10 and 15 cm of the cardiac region of the thorax.

Our segmentation technique has been tested in several ways. First, we checked whether the algorithm was able to deliver any segmentation result for a selected vessel and a user defined start and end point. That aimed on investigating its capability to work on data sets with breathing artifacts being present. An acceptable segmentation result could be obtained in all cases where the continuity of the vessel between the slices of the data set was given. If the breathing of the patient led to too strong artifacts in the image data resulting in a loss of connectivity on the voxel level, the initial path could not be continued until it reached the end point. Thus, the segmentation failed in those cases resp. only a part of the vessel could be segmented. These tests delivered 27 extracted coronary arteries resp. segments of them that have been further investigated for evaluating the quality of the segmentation.

The accuracy of the border point detection has been evaluated by the means of 2D slices with highlighted pixels according to the computed coordinates. Due to the fact that the coronary arteries appear only a few pixels large in the slices, the data has been magnified by a factor of 3 (no interpolation applied). That allowed a more accurate investigation of the computed border points, since these values were computed on a floating point basis. The correctness of the calculated positions was quite satisfying. In most of the cases the highlited pixels
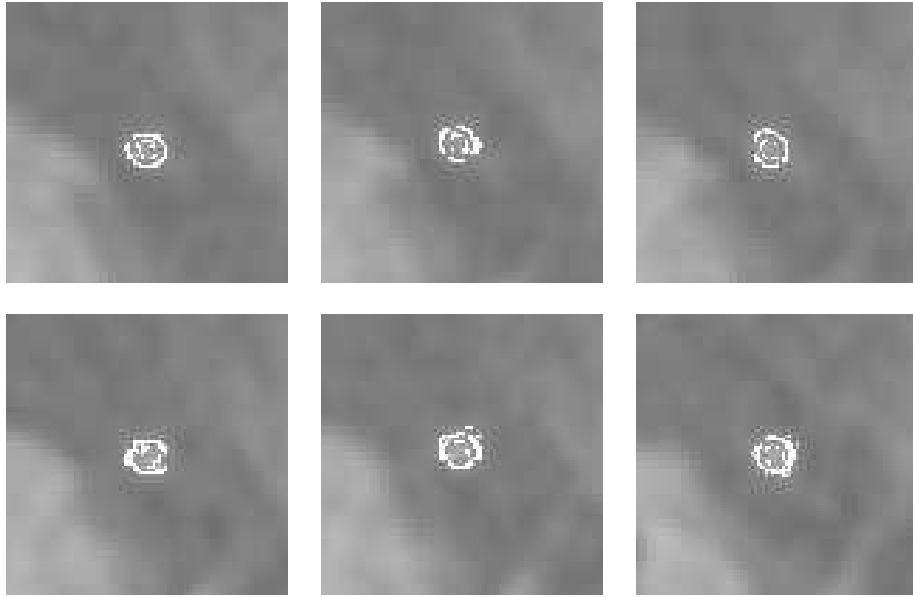
Figure 5. The computed border position of the vessel. The border points are highlighted, and the axial slices have been magnified by a factor of 3 for a better visibility.

lay at positions which coincided quite well with the vessel's border. However, there was often a 'one-pixel-shift' or a double border. Figure 5 shows an exemplary result of the border detection.

The border points did not form a closed curve; single dots could be perceived. But, this is not considered to be a problem, since the medical application we are focusing on, requires a highlighting of the vessel together with the 3D rendered volume. That is done based on the creation of polygonal meshes, which does not require closed curves or even smooth surfaces to work with.

One of the design constraints for the algorithm was the exclusion of calcifications from the segmentation output. We tested whether this demand was fulfilled by examining 3D rendered scenes of the data. In most of the cases the generated border did not include calcified regions, but in some of them – especially when the calcification was bound to a curve of the coronary artery – the border points slightly surrounded the calcification. Figure 6 shows results for calcified regions where that 'surrounding' appeared. In figure 7 the segmentation result for a longer segment is visualized in a 3D scene containing the volume rendered data and the segmented border of the coronary artery. The latter one is displayed as a polygonal mesh created from the border points using a marching cubes algorithm.[17]

Executing our segmentation technique, the centerline was corrected iteratively in combination with the detection of the vessel's border. We investigated the number of iterations that are required to bring that points in a centered position with respect to the coronary artery. That centering is not only dependent from the number of iterations, but also from the number of rays along those the border is searched. A number of only 4 rays could not reliably center the path. For our investigation we used 512 rays and found a number of 8 iterations to be sufficient for computing the 'real' centerline (see figure 8).

As a further test of the capabilities of the segmentation algorithm we calculated the vessel's mean diameter based on the centerline points and those of the extracted border. An exemplary output of the generated graph is shown in figure 9. The diameter of the segmented coronary artery has been determined to be approx. $2\,mm$, which is a typical size for such a vessel.

The segmentation part of the algorithm (steps 2 and 3) turned out to be fast, it was done in less than 10 seconds on current PC hardware (Dual *Athlon MP 1800+*, Windows 2000; *nVidia GeForce 3* graphics board). The most time-consuming issue was the pre-processing of the data, and there above all the median filtering.
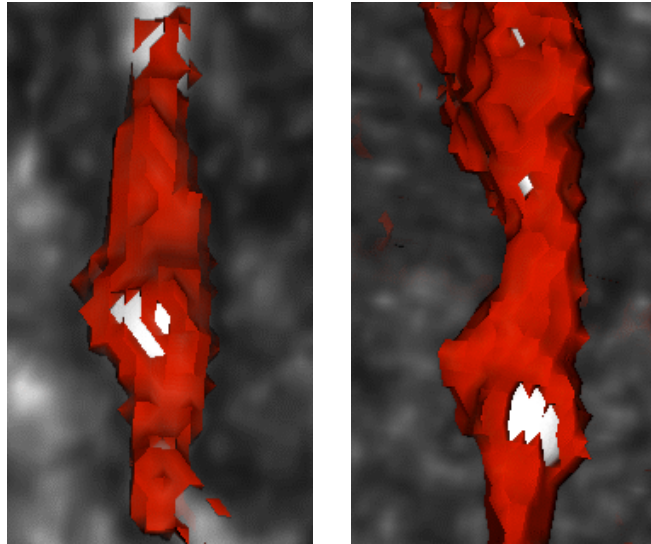
Figure 6. Results concerning the correct handling of calcifications. An exclusion of the calcification from the segmented region was difficult for some data sets. Here, two vessels are shown where the calcification is slightly surrounded by the generated border and not completely excluded from the segmentation result.

Figure 7. A volume rendered CT data set with a segmented coronary artery. The vessel's border is represented by a polygonal mesh (red) created from the computed border points. Three calcifications (a large one and two smaller ones) can be perceived. They have been excluded from the segmented region.
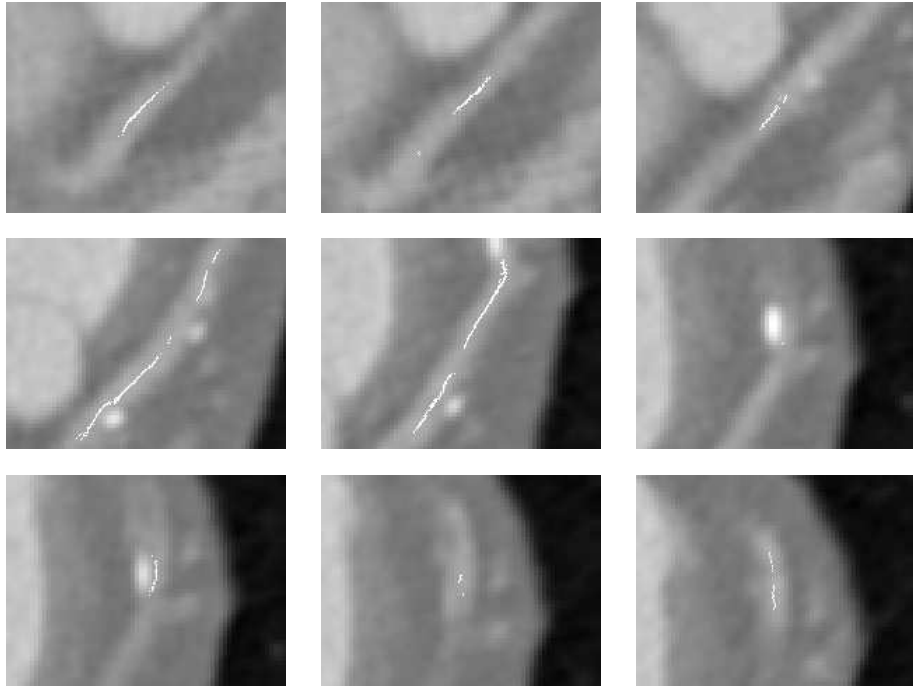
Figure 8. The computed centerline of a coronary artery. Nine axial slices containing the highlighted points of the segmented path are shown. The centerline is smoothly passing by the calcification in the lower left slice. (Due to the vessel's course nearly parallel to the images plane of the first slices, the path seems to 'disappear' sometimes. But in reality it is a continous line without interruptions.)
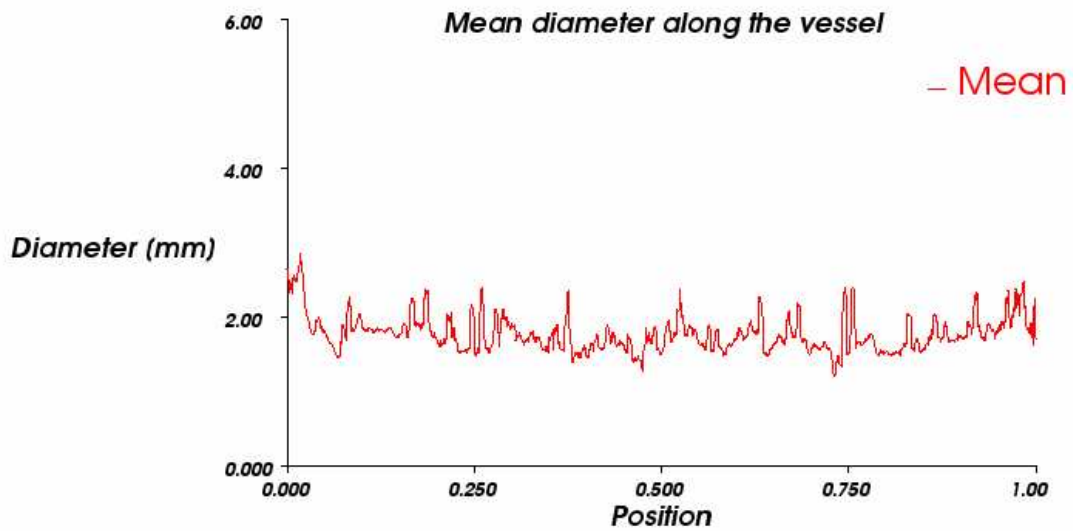

Figure 9. The mean diameter of a segmented coronary artery. This graph has been created from the two point lists generated by the algorithm representing the centerline and the border.

6. DISCUSSION

As the major drawback of the algorithm presented in this work one might consider the fact that the computed border points neither form a smooth surface in 3D nor a closed curve in planes perpendicular to the centerline. This is due to the simple cost function we have used for deciding whether a ray should be stopped. A subsequent smoothing of the computed border points could improve that segmentation result, but it has not yet been investigated. Future work will focus on that 'border problem' incorporating the work of Hildebrand et al.[18] and Verdonck et al..[13] The cost functions that they employed seems to be more suitable for the border point detection problem. An advantage of our approach is the fact, that these cost functions can easily be included into our technique, since we have used that 'three-step' technique presented in section 4.

However, even though the iterative correction of the centerline was based on that simple detection scheme, it was very satisfying. The centerline followed the central axis of the segmented coronary arteries, and always passed an existing calcification on the 'right' side. Based on the two point lists that represent the output of the segmentation we could show, that a reliable calculation of the vessel's diameter is possible (see also reference[7]). The usefullness of that parameter extraction will even increase with the improved border detection we intend to integrate. This will allow further examinations of the segmented coronary arteries comparable with the investigation of tracheal stenoses as published by Sorantin et al..[14]

Despite the weaknesses of our approach discussed above, it will be used in the medical application it has been designed for. The TECAB grafting requires a knowledge about the location of a coronary artery with respect to the surrounding tissue. It has to be known whether it is surrounded by fat or freely accessible on the heart's surface. This decision can be made very well even if the computed points do not exactly coincide with the vessel's border. For the support of the port placement, this problem can actually be neglected since an augmented view provided by our MEDARPA[2] system will include a polygon-based representation of the coronary artery, and for that application the accuracy is sufficient.

Future work will also include a more sophisticated filtering in order to decrease the pre-processing time. There, we will restrict the application of the filters to a user defined region of interest.

7. CONCLUSION AND OUTLOOK

We have presented a new method for the segmentation of vessels, called the 'corkscrew algorithm'. It has been designed for the segmentation of coronary arteries in contrast-enhanced CT data sets. The algorithm's ability to extract vessels has been investigated showing satisfying results. Weaknesses of the extraction technique and possibilities to overcome these problems have been discussed.

The usabilty of our algorithm for the intended use with the TECAB grafting has been evaluated. It will provide additional information for the planning and execution of that intervention. Based on the segmentation results further parameters describing the vessel's morphology will be extracted.

ACKNOWLEDGMENTS

REFERENCES

1. S. Dogan, G. Wimmer-Greinecker, E. Andreen, S. Mierdl, K. Westphal, and A. Moritz, "Totally Endoscopic Coronary Artery Bypass (TECAB) Grafting and Closure of an Atrial Septal Defect using the DaVinci System," *Journal of Thoracic and Cardiovascular Surgery* **48**, 2000.
2. "Medarpa." http://www.medarpa.de, 2003.
3. M. Schnaider, B. Schwald, H. Seibert, and T. Weller, "Medarpa - A Medical Augmented Reality System for Minimal-Invasive Interventions," in *Proceedings of the 11th Annual Medicine Meets Virtual Reality (MMVR) Conference*, (Newport Beach, CA, USA), January 2003.

4. B. Schwald, H. Seibert, and T. Weller, "A Flexible Tracking Concept Applied to Medical Scenarios Using an AR Window," in *International Symposium on Mixed and Augmented Reality (ISMAR'02)*, (Darmstadt, Germany), September 2002.

5. S. Wesarg, "MEDARPA MEDical Augmented Reality for PAtients, CG topics 1/2002," *Reports of the House of Computer Graphics, Darmstadt, Germany* **14**, p. 5, 2002.

6. S. Wesarg, E. A. Firle, B. Schwald, H. Seibert, P. Zogal, and S. Röddiger, "Accuracy of needle implantation in brachytherapy using a medical AR system – a phantom study," *Proc. of SPIE Medical Imaging*, 2004.

7. S. Wesarg and E. A. Firle, "Localizing Calcifications in Cardiac CT Data Sets Using a New Vessel Segmentation Approach," in *Society for Computer Applications in Radiology, Proc. of the 21st Meeting*, 2004.

8. C. Kirbas and K. H. Quek, "A Review of Vessel Extraction Techniques and Algorithms." available online: `http://vislab.cs.wright.edu/review/Extraction/extractionReview.pdf`, November 2002.

9. D. L. Parker, J. Wu, and R. E. van Bree, "Three dimensional vascular reconstruction from projections: A theoretical overview," in *Engineering in Medicine and Biology Society, Proc. of the Annual International Conference of the IEEE* **1**, pp. 399–400, 1988.

10. F. Mao, S. Ruan, A. Bruno, C. Toumoulin, R. Collorec, and P. Haigron, "Extraction of structural features in digital subtraction angiography," in *Biomedical Engineering Days, Proc. of the 1992 International*, pp. 166–169, 1992.

11. T. Tozaki, Y. Kawata, N. Niki, H. Ohmatsu, and N. Moriyama, "3-d Visualization of Blood Vessels and Tumor Using Thin Slice CT Images," in *Nuclear Science Symposium and Medical Imaging Conference, Proc. of IEEE* **3**, pp. 1470–1474, 1995.

12. W. E. Higgins, W. J. T. Spyra, and E. L. Ritman, "Automatic Extraction of the Arterial Tree from 3-D Angiograms," in *Engineering in Medicine and Biology Society, Proc. of the 11th Annual International IEEE Conference* **2**, pp. 563–564, November 1989.

13. B. Verdonck, I. Bloch, H. Maître, D. Vandermeulen, P. Suetens, and G. Marchal, "Blood Vessel Segmentation and Visualization in 3D MR and Spiral CT Angiography," in *Computer Assisted Radiology*, H. U. Lemke, ed., *Proc. of the CAR 1995*, pp. 177–182, Springer, 1995.

14. E. Sorantin, C. Halmai, B. Erdöhely, K. Palágyi, L. G. Nyúl, K. Ollé, B. Geiger, F. Lindbichler, G. Friedrich, and K. Kiesler, "Spiral-CT-Based Assessment of Tracheal Stenoses Using 3-D-Skeletonization," *IEEE Transactions on Medical Imaging* **21**, pp. 263–273, March 2002.

15. Y. Kawata, N. Niki, and T. Kumazaki, "An Approach for Detecting Blood Vessel Diseases from Cone-Beam CT Image," in *International Conference on Image Processing, Proc. of IEEE* **2**, pp. 500–503, October 1995.

16. N. Armande, P. Montesinos, O. Monga, and G. Vaysseix, "Thin Nets Extraction Using a Multi-scale Approach," *Computer Vision and Image Understanding: CVIU* **73**(2), pp. 248–257, 1999.

17. W. Schroeder, K. Martin, and B. Lorensen, *The Visualization Toolkit – An Object-Oriented Approach to 3D Graphics*, Kitware, Inc., 3rd ed., 2002.

18. A. Hildebrand and S. Großkopf, "3D Reconstruction of Coronary Arteries from X-Ray Projections," in *Computer Assisted Radiology*, H. U. Lemke, ed., *Proc. of the CAR 1995*, Springer, 1995.